Figure S1

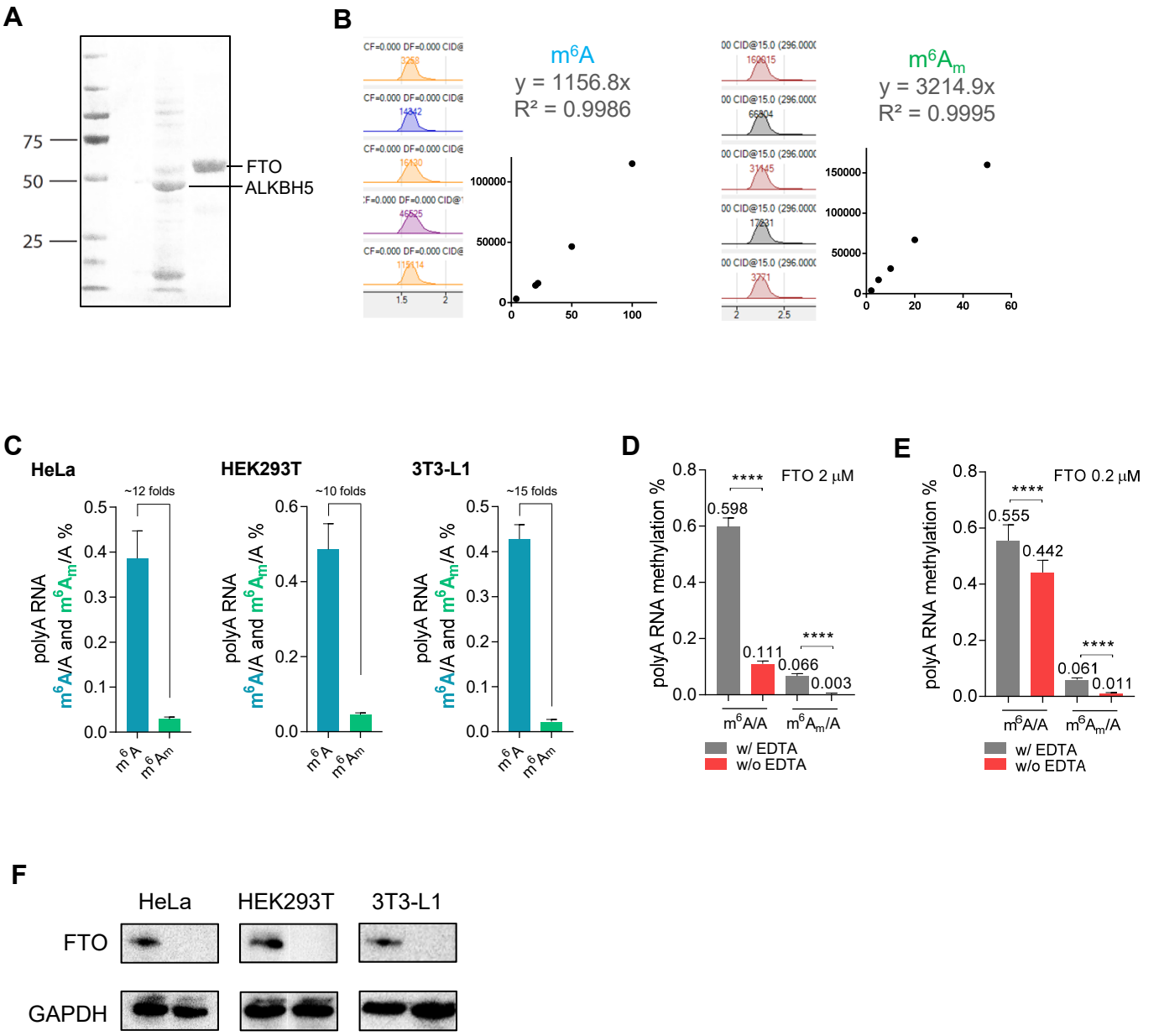
A
75
50
25
FTO
ALKBH5
B
m6A
y = 1156.8x
R² = 0.9986
m6Am
y = 3214.9x
R² = 0.9995
C
HeLa
HEK293T
3T3-L1
~12 folds
~10 folds
~15 folds
polyA RNA m6A/A and m6Am/A %
m6A
m6Am
D
FTO 2 μM
polyA RNA methylation %
0.598
0.111
0.066
0.003
****
m6A/A
m6Am/A
w/ EDTA
w/o EDTA
E
FTO 0.2 μM
0.555
0.442
0.061
0.011
F
HeLa
HEK293T
3T3-L1
FTO
GAPDH

Figure S1. FTO Demethylates Both Internal m^6A and Cap m^6A_m *in vitro*, Related to Figure 1.

(A) Coomassie blue analysis of purified mammalian FTO.

(B) Left: LC-MS/MS channel, peak area and standard curve for the m^6A modification; Right: LC-MS/MS channel, peak area and standard curve for the m^6A_m modification.

(C) Quantification of the m^6A/ m^6A_m ratio in HeLa, HEK293T and 3T3-L1 cells by LC-MS/MS, showing that the m^6A to m^6A_m ratios are consistently around 10-fold in HeLa, HEK293T, and 3T3-L1 cells.

(D) and (E) Quantification of methylation percentage of the m^6A/A ratio and the m^6A_m/A ratio by LC-MS/MS *in vitro*. (D) Incubated with 200 ng purified polyadenylated RNA from HEK293T cells for 1 h under the reported demethylation conditions: 2 μM recombinant FTO in the 20 μl solution was able to demethylate ~81% internal m^6A and ~95% cap m^6A_m; (E) Incubated with 200 ng purified polyadenylated RNA from HEK293T cells for 1 h under the reported demethylation conditions: 0.2 μM recombinant FTO in the 20 μl solution was able to demethylate ~20% internal m^6A and ~82% cap m^6A_m.

(F) Western blot of the knockdown of FTO in HeLa, HEK293T and 3T3-L1 cells. *P* values were determined using Student's t-test. *$p < 0.05$, **$p < 0.01$, ***$p < 0.001$, ****$p < 0.0001$. *n.s*. means not significant. Error bars, mean ± s.d. for $n = 6$ experiments in (C) to (E).

Figure S2

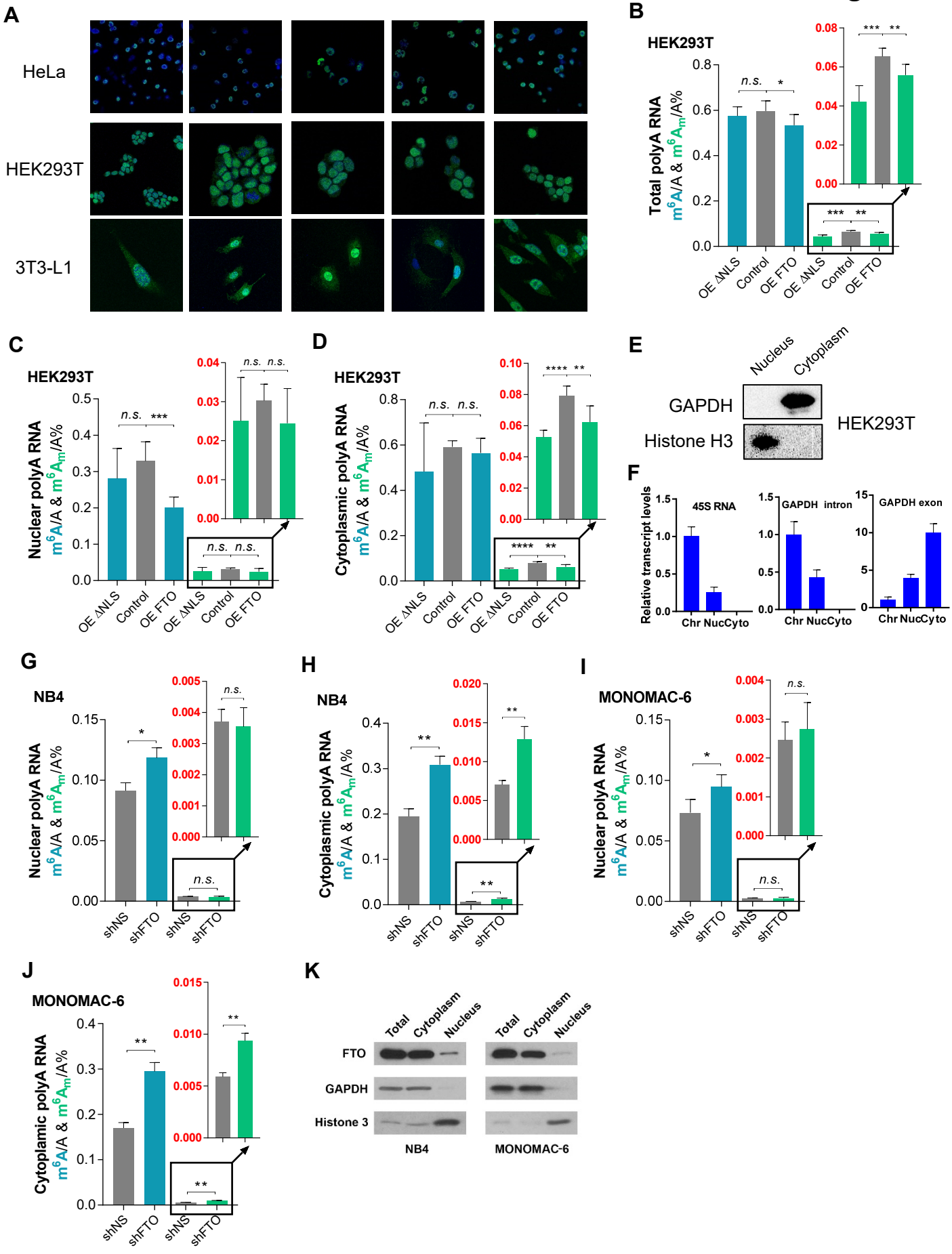
A
HeLa
HEK293T
3T3-L1
B
HEK293T
Total polyA RNA
m6A/A & m6Am/A%
n.s.
*
***
**
OE ΔNLS
Control
OE FTO
C
HEK293T
Nuclear polyA RNA
m6A/A & m6Am/A%
n.s.
***
D
HEK293T
Cytoplasmic polyA RNA
m6A/A & m6Am/A%
****
E
Nucleus
Cytoplasm
GAPDH
Histone H3
HEK293T
F
Relative transcript levels
45S RNA
GAPDH intron
GAPDH exon
Chr
NucCyto
G
NB4
Nuclear polyA RNA
m6A/A & m6Am/A%
shNS
shFTO
H
NB4
Cytoplasmic polyA RNA
m6A/A & m6Am/A%
I
MONOMAC-6
Nuclear polyA RNA
m6A/A & m6Am/A%
J
MONOMAC-6
Cytoplamic polyA RNA
m6A/A & m6Am/A%
K
Total
Cytoplasm
Nucleus
FTO
GAPDH
Histone 3
NB4
MONOMAC-6

Figure S2. FTO Differentially Mediates Internal m^6A or Cap m^6A_m Demethylation in the Polyadenylated RNA in the Nucleus and the Cytoplasm, Related to Figure 2.

(A) Five representative immunofluorescent pictures of the endogenous FTO in HeLa, HEK293T and 3T3-L1 cells.

(B) to (D) Quantification of the m^6A/A ratio (blue bars) and the cap m^6A_m/A ratio (green bars) in the polyadenylated RNA from HEK293T cells by LC-MS/MS. In comparison to the control: (B) the overexpression of the wild-type FTO but not the ΔNLS-FTO (FTO without nuclear localization signal) led to significant decreases of the m^6A/A ratio in the total polyadenylated RNA; while the overexpression of both the ΔNLS-FTO and the wild-type FTO led to noticeable decreases of the m^6A_m/A ratio in the total polyadenylated RNA; (C) overexpression of wild-type FTO led to a significant decrease of the m^6A/A ratio but not the m^6A_m/A ratio in the nuclear polyadenylated RNA, while the overexpression of ΔNLS-FTO did not result in significant decreases in the m^6A/A or the m^6A_m/A ratios in the nuclear polyadenylated RNA; (D) the overexpression of both the ΔNLS-FTO and the wild-type FTO led to a significant decrease of the m^6A_m/A ratio but not the m^6A/A ratio in the cytoplasmic polyadenylated RNA.

(E) Western blot validation of cytoplasm and nucleus separation in HEK293T cells.

(F) qRT-PCR validation of cytoplasm and nucleus separation in HEK293T cells.

(G) and (H) Quantification of the m^6A/A ratio (blue bars) and the cap m^6A_m/A ratio (green bars) in the polyadenylated RNA from NB4 cells by LC-MS/MS. Stable knockdown of FTO led to (G) the increased m^6A/A ratio but not the cap m^6A_m/A ratio in the nuclear polyadenylated RNA and (H) both increased m^6A/A ratio and the cap m^6A_m/A ratio in the cytoplasmic polyadenylated RNA.

(I) and (J) Quantification of the m^6A/A ratio (blue bars) and the cap m^6A_m/A ratio (green bars) in polyadenylated RNA from MONOMAC-6 cells by LC-MS/MS. Stable knockdown of FTO led to (I) the increased m^6A/A ratio but not the cap m^6A_m/A ratio in the nuclear polyadenylated RNA and (J) both increased m^6A/A and the cap m^6A_m/A ratios in the cytoplasmic polyadenylated RNA.

(K) Western blot of the FTO in total, cytoplasm and nucleus in NB4 and MONOMAC-6 cells. *P* values were determined using Student's t-test. *$p < 0.05$, **$p < 0.01$, ***$p < 0.001$, ****$p < 0.0001$. *n.s.* means not significant. Error bars, mean ± s.d. for $n = 6$ experiments in (B) to (D); for $n = 4$ experiments in (G) to (J).

Figure S3

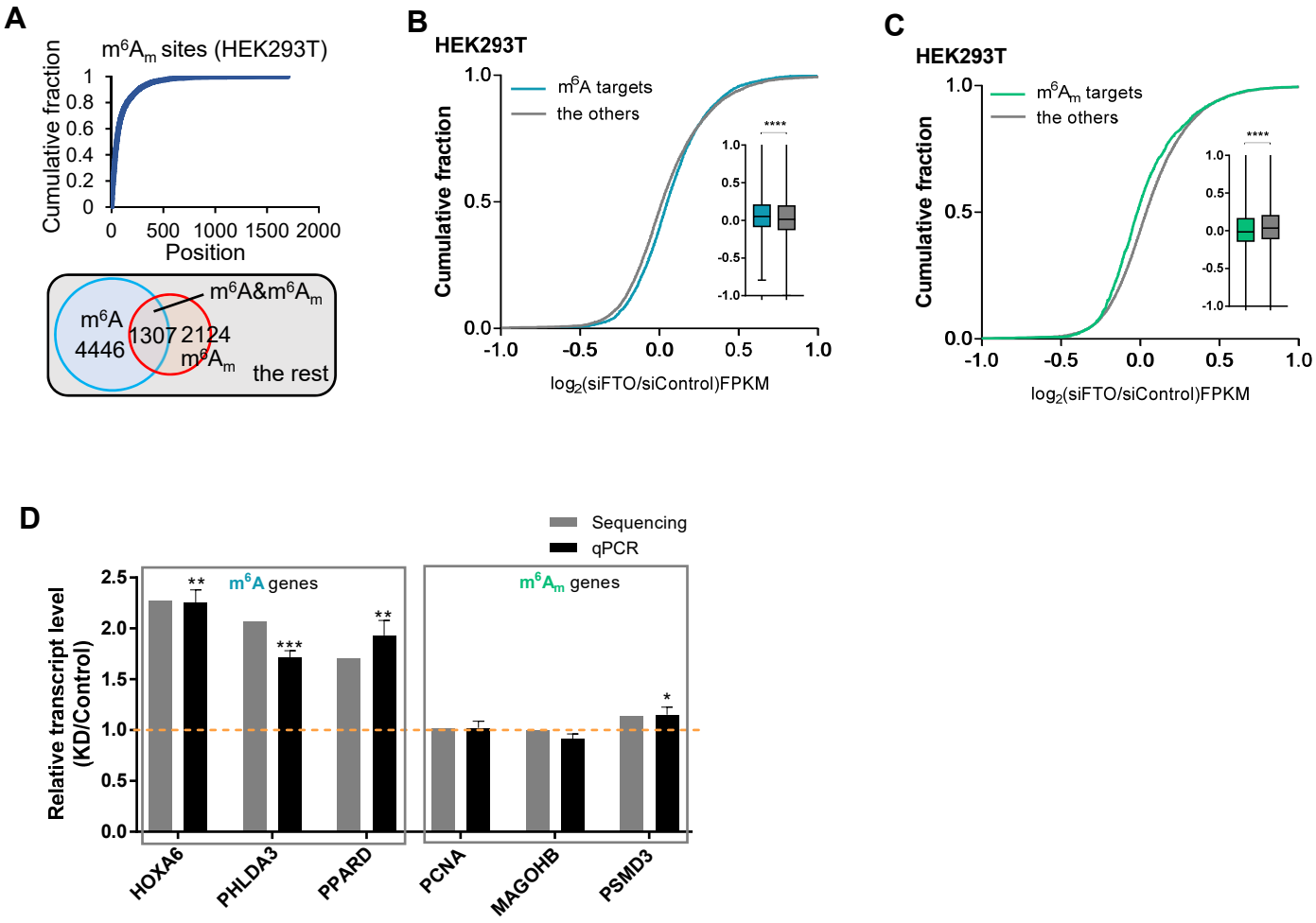
A
m6Am sites (HEK293T)
Cumulative fraction
Position
m6A
4446
1307
2124
m6Am
m6A&m6Am
the rest
B
HEK293T
m6A targets
the others
Cumulative fraction
log2(siFTO/siControl)FPKM
****
C
HEK293T
m6Am targets
the others
Cumulative fraction
log2(siFTO/siControl)FPKM
****
D
Sequencing
qPCR
Relative transcript level (KD/Control)
m6A genes
m6Am genes
HOXA6
PHLDA3
PPARD
PCNA
MAGOHB
PSMD3

Figure S3. Dynamic Regulation of m^6A but not Cap m^6A_m Influences mRNA Transcript Levels, Related to Figure 3.

(A) Cumulative fraction of the m^6A_m sites along mRNA beginning with the transcription start site (top). Scheme for the transcripts grouping method (bottom).

(B) mRNAs were classified into the transcripts containing only internal m^6A and the rest as control. In HEK293T cells, FTO knockdown led to a significant increased global transcript level changes of the transcripts containing only m^6A (n = 3987, m^6A only; n = 8921, the rest).

(C) mRNAs are classified into the transcripts containing cap m^6A_m only and the rest as control. In HEK293T cells, compared to the transcripts that do not contain m^6A_m, FTO knockdown led to a significantly less global transcript level changes of the transcripts containing only m^6A compared to the rest (n = 1885, m^6A only; n = 11023, the rest). P values were determined using Mann-Whitney test. *p < 0.05, **p < 0.01, ***p < 0.001, ****p < 0.0001. *n.s.* means not significant. Error bars, mean ± s.d. in (B) and (C). Data represent the average from two independent mRNA expression datasets; each box shows the first quartile, median, and third quartile.

(D) qRT-PCR validation of transcript level changes of three genes containing only m^6A and three genes containing only m^6A_m. *p < 0.05, **p < 0.01, ***p < 0.001, ****p < 0.0001. *n.s.* means not significant. Error bars, mean ± s.d. for n = 6 experiments in (D).

Figure S4

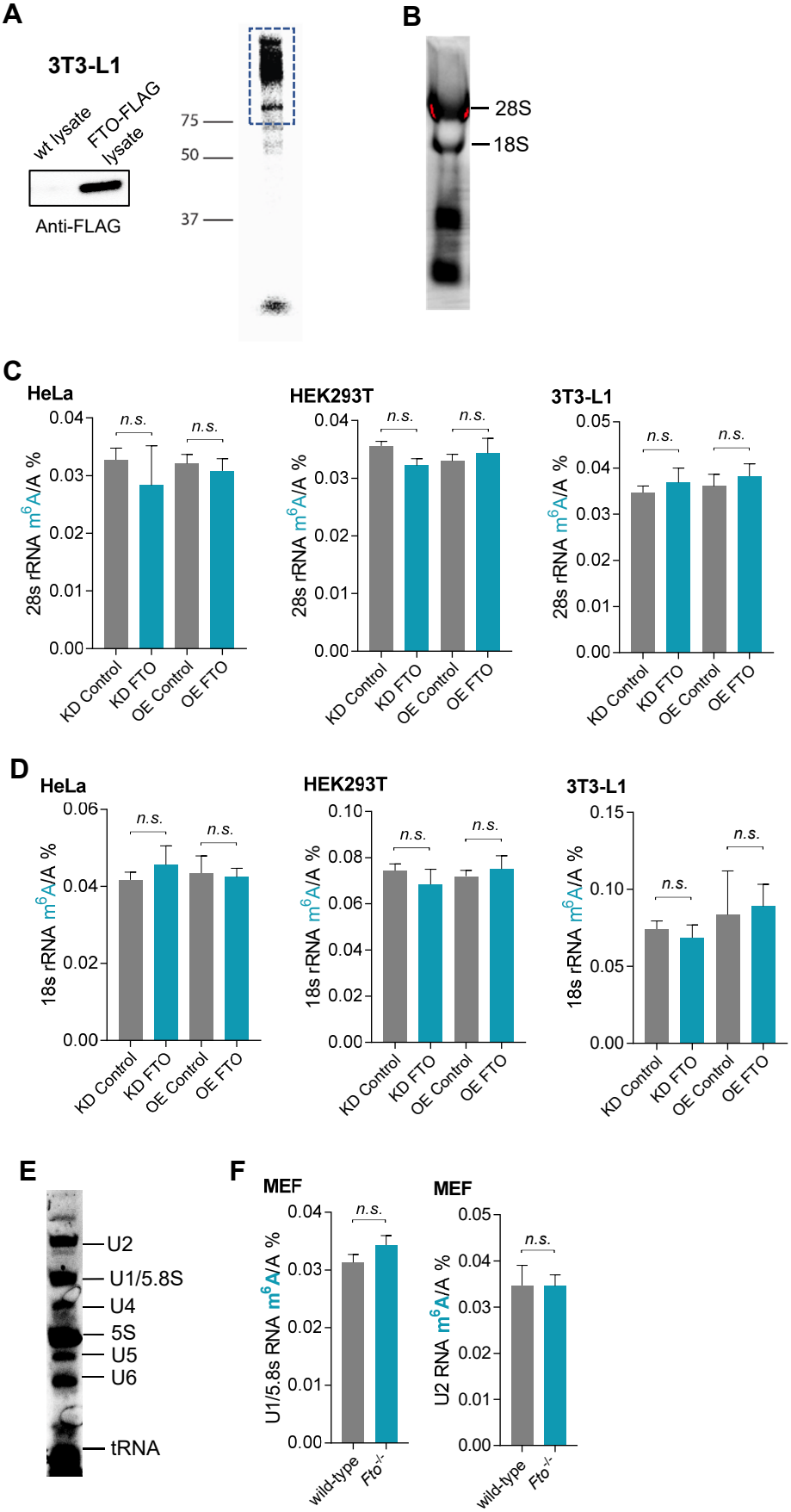
A
3T3-L1
wt lysate
FTO-FLAG lysate
Anti-FLAG
75
50
37
B
28S
18S
C
HeLa
HEK293T
3T3-L1
28s rRNA m6A/A %
n.s.
KD Control
KD FTO
OE Control
OE FTO
D
HeLa
HEK293T
3T3-L1
18s rRNA m6A/A %
n.s.
KD Control
KD FTO
OE Control
OE FTO
E
U2
U1/5.8S
U4
5S
U5
U6
tRNA
F
MEF
U1/5.8s RNA m6A/A %
MEF
U2 RNA m6A/A %
n.s.
wild-type
Fto-/-

Figure S4. Quantification of the m^{6}A Level Changes inside Cell in the FTO-Associated RNA Species, Related to Figure 4.

(A) Left: Western blot validation of anti-FLAG pulldown purity; right: SDS-PAGE protein gel of ^{32}P labeled FTO-nucleic acids complex.

(B) Separation of 28S rRNA and 18S rRNA from total RNA shown on a 2% agarose gel.

(C) and (D) Quantification of the m^{6}A/A ratio in rRNA by LC-MS/MS. In comparison to the control, no obvious changes of m^{6}A/A ratio (C) in 28S rRNA or (D) in 18S rRNA were observed in HeLa, HEK293T, and 3T3-L1 cell lines upon the alterations of FTO expression.

(E) Separation of individual snRNAs from the purified nuclear RNA below 200 nucleotides shown on the 6% TEB-Urea gel.

(F) Quantification of the m^{6}A/A ratio in U1/5.8s RNA and U2 RNA by LC-MS/MS. No obvious change was observed in the Fto knockout MEF cells compared to the wild-type control. *$p < 0.05$, **$p < 0.01$, ***$p < 0.001$, ****$p < 0.0001$. *n.s.* means not significant. Error bars, mean ± s.d. for $n = 3$ experiments in (C) and (D); and for $n = 6$ experiments in (F).

Figure S5

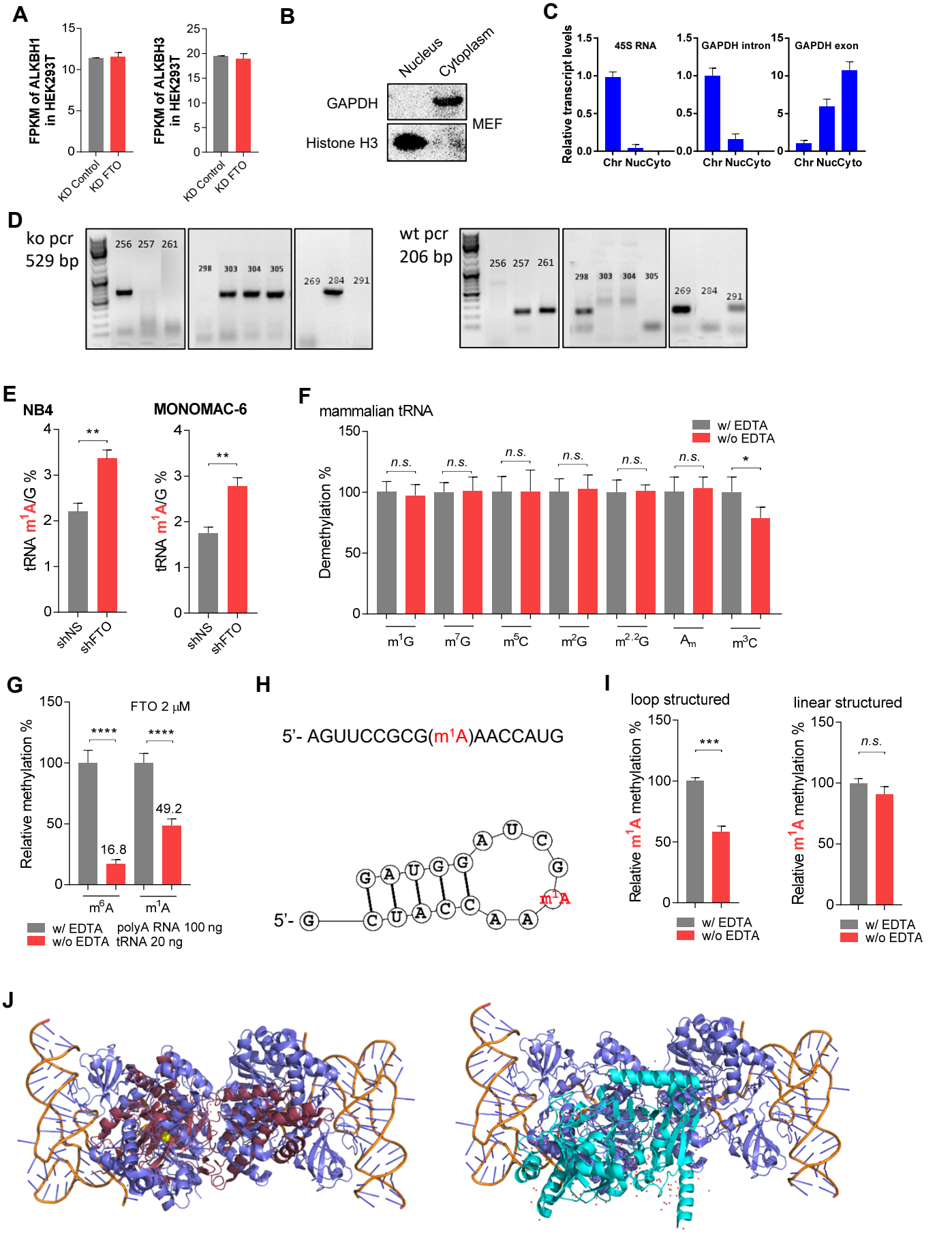
A
FPKM of ALKBH1 in HEK293T
FPKM of ALKBH3 in HEK293T
KD Control
KD FTO
B
Nucleus
Cytoplasm
GAPDH
Histone H3
MEF
C
Relative transcript levels
45S RNA
GAPDH intron
GAPDH exon
Chr NucCyto
D
ko pcr
529 bp
wt pcr
206 bp
256 257 261
298 303 304 305
269 284 291
E
NB4
MONOMAC-6
tRNA m1A/G %
shNS
shFTO
F
mammalian tRNA
w/ EDTA
w/o EDTA
Demethylation %
n.s.
m1G
m7G
m5C
m2G
m2,2G
Am
m3C
G
FTO 2 μM
Relative methylation %
16.8
49.2
m6A
m1A
w/ EDTA polyA RNA 100 ng
w/o EDTA tRNA 20 ng
H
5'- AGUUCCGCG(m1A)AACCAUG
5'-
I
loop structured
linear structured
Relative m1A methylation %
w/ EDTA
w/o EDTA
J

Figure S5. Quantification of m^1A Level Changes in AML cells, Control Experiments for tRNA m^1A Demethylation, and Structure Correlation of FTO with tRNA, Related to Figure 5.

(A) Relative gene expression of ALKBH1 and ALKBH3 from RNA-seq in the HEK293T cells upon the knockdown of FTO. NO changes were observed for both ALKBH1 and ALKBH3.

(B) Western blot validation of cytoplasm and nucleus separation in MEF cells.

(C) qRT-PCR validation of cytoplasm and nucleus separation in MEF cells.

(D) PCR validation for *Fto*$^{-/-}$ and wild-type mouse.

(E) Quantification of the m^1A/G ratio in tRNA, showing the increased m^1A/G in NB4 and MONOMAC-6 cells upon stable FTO knockdown.

(F) Demethylation of total tRNA isolated from HEK293T cells by mammalian FTO *in vitro*. Slightly decrease of m^3C/G ratio can be observed but no obvious changes of m^1G/G, m^7G/G, m^5C/G, m^2G/G, $m^2{}_2G/G$, or A_m/G ratios can be observed.

(G) Demethylation of total tRNA and polyadenylated RNA isolated from HEK293T cells by mammalian FTO *in vitro*. With the similar numbers of m^1A and m^6A molecule, the demethylation activity towards m^1A is slightly lower than m^6A.

(H) Sequence of the linear ssRNA probe containing m^1A (top); sequence of the loop-structured ssRNA probe containing m^1A and predicted structure by RNA fold server (http://rna.tbi.univie.ac.at/cgi-bin/RNAWebSuite/RNAfold.cgi).

(I) FTO exhibits m^1A demethylation activity preferentially in the loop structure revealed by *in vitro* demethylation assays with m^1A in a linear ssRNA probe and m^1A in a stem-loop structured probe.

(J) Left: overlapped structures of FTO (raspberry) with the complex of NSUN6 (purple) and tRNA (orange). The iron center of FTO is depicted in yellow ball; right: overlapped structures of ALKBH5 (green) with the complex of NSUN6 (purple) and tRNA (orange). *P* values were determined using Student's t-test. *p < 0.05, **p < 0.01, ***p < 0.001, ****p < 0.0001. *n.s.* means not significant. Error bars, mean ± s.d. for $n = 3$ experiments in (F), (G), and (I); for $n = 4$ experiments in (E).

Figure S6

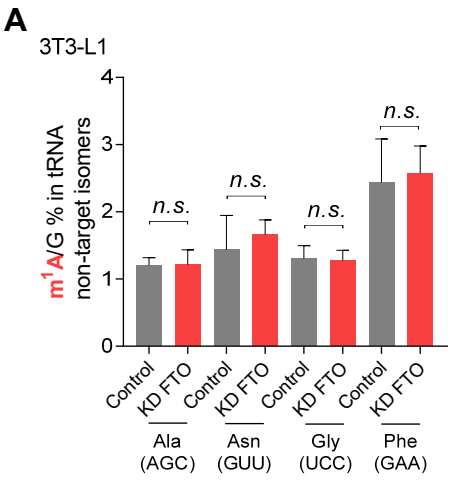
A
3T3-L1
m1A/G % in tRNA non-target isomers
n.s.
n.s.
n.s.
n.s.
Control
KD FTO
Ala (AGC)
Asn (GUU)
Gly (UCC)
Phe (GAA)

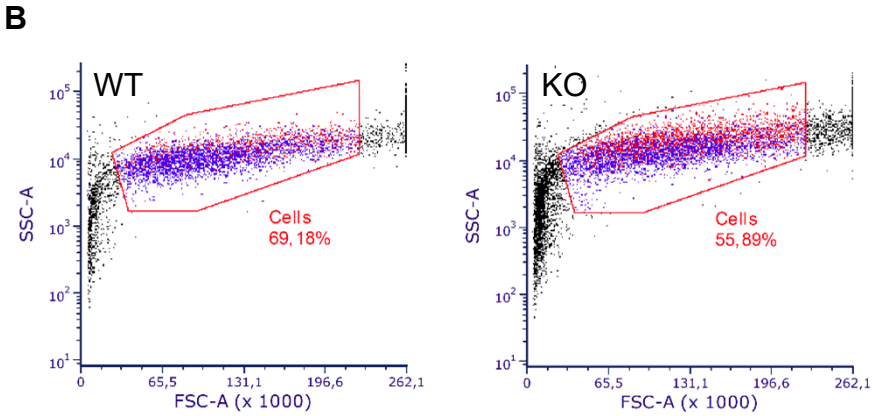
B
WT
KO
SSC-A
FSC-A (x 1000)
Cells
69,18%
55,89%

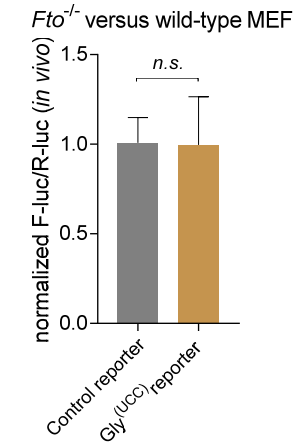
C
Fto-/- versus wild-type MEF
normalized F-luc/R-luc (in vivo)
n.s.
Control reporter
Gly(UCC) reporter

Figure S6. Quantifications of m^1A Level Changes in Non-Bound Individual tRNAs and Control Experiments for Translation Regulation, Related to Figure 6.

(A) Quantification of the m^1A/G ratio in several non-CLIP tRNAs by LC-MS/MS. In comparison to the control, no obvious changes of m^1A/G ratios in $tRNA^{Ala(AGC)}$, $tRNA^{Asn(GUU)}$, $tRNA^{Gly(UCC)}$, and $tRNA^{Phe(GAA)}$ can be observed. *P* value was determined using Student's t-test. *p < 0.05, **p < 0.01, ***p < 0.001, ****p < 0.0001. *n.s.* means not significant. Error bars, mean ± s.d. for $n = 3$ experiments.

(B) The flow-cytometry (FACS) gating strategy applied to wild-type (left) and *Fto*$^{-/-}$ (right) MEF cells.

(C) The effects of non-targets $tRNA^{Gly(UCC)}$ was revealed by the reporter assay, showing no noticeable increase of protein synthesis in *Fto*$^{-/-}$ MEF cell compared to the wild-type MEF cell. *P* value was determined using Student's unpaired t-test. *p < 0.05, **p < 0.01, ***p < 0.001, ****p < 0.0001. *n.s.* means not significant. Error bars, mean ± s.d. for $n = 8$ experiments in (C).

Table S4. Biotinylated single-stranded DNA probes designed to isolate specific tRNAs, related to Figure 6

$tRNA^{Glu(CUC)}$	5’biotin-TTCCCTGACCGGGAATCGAACCCGGGCCG
$tRNA^{His(GUG)}$	5'-biotin-TGCCGTCACTCGGATTCGAACCGAGGTTGCTG
$tRNA^{Gly(GCC)}$	5'biotin-TGCATTGGCCGGGAATCGAACCCGGGGCCTC
$tRNA^{Asp(GUC)}$	5'biotin-CTCCCCGTCGGGGAATCGAACCCCGGTCTC
$tRNA^{Lys(CUU)}$	5’biotin-CCAACGTGGGGCTCGAACCCACGACCCT
$tRNA^{Gln(CUG)}$	5’biotin-AGGTCCCACCGAGATTTGAACTCGGATCGCTGG
$tRNA^{Leu(CAA)}$	5’biotin- TGTCAGAAGTGGGATTCGAACCCACGCCT
$tRNA^{Ala(AGC)}$	5’biotin-TGGAGGATGCGGGCATCGATCCCGCTACC
$tRNA^{Asn(GUU)}$	5’biotin-CGTCCCTGGGTGGGCTCGATCCACCAACC
$tRNA^{Gly(UCC)}$	5’biotin- TGCGTTGGCCGGGAATCGAACCCGGGTCAAC
$tRNA^{Phe(GAA)}$	5’biotin-TGCCGAAACCCGGGATCGAACCAGGGAC